

Cite this: *Dalton Trans.*, 2024, **53**, 17207

Polyoxometalate-supported transition metal complexes for the oxidative cross-coupling of amines and alcohols†

Ankita Pardiwala, Meghal A. Desai  and Ritambhara Jangir *

Three new hybrid polyoxometalates (POMs) based on transition metals, namely, copper metal with γ -[Mo₈O₂₆]⁴⁻ polyoxometalates [Cu(DMF)₄(Mo₈O₂₆)·2C₃H₈NO]·1.8 DMF (**1**), cobalt metal with hexamolybdate [Co(DMSO)₆][Mo₆O₁₉] (**2**), and nickel metal with hexamolybdate [Ni(DMSO)₆][Mo₆O₁₉] (**3**), were developed. These materials were characterised by applying both analytical and spectroscopic techniques (IR, TGA, and CHNO elemental analysis), and structural elucidation was performed using single-crystal X-ray diffraction studies. Among these hybrid POMs, octamolybdate with copper was used for the catalytic production of benzimidazoles. The incorporation of [Cu(DMF)₄] between two octamolybdates results in the transformation of POMs into a useful catalyst, which effectively catalyses the oxidative cross-coupling of anilines, benzyl alcohol, and sodium azide to produce benzimidazole. This catalytic reaction occurs in the presence of *tert*-butyl hydroperoxide (TBHP) at a moderate temperature. Benzimidazole and its derivatives are highly preferred owing to their wide-ranging biological activities and clinical applications. These compounds are exceptionally effective in terms of their selectivity ratio and inhibitory activity. The catalytic reaction presented herein is a one-pot procedure that includes a series of reactions, such as C–H functionalization, condensation, *ortho* selective amination, and cyclization.

Received 10th August 2024,
Accepted 19th September 2024

DOI: 10.1039/d4dt02289k

rsc.li/dalton

1. Introduction

Research on the implementation of affordable and environmentally friendly catalysts has grown significantly. In the meantime, polyoxometalates (POMs) are gaining popularity for their remarkable stability, ease of production, and nanostructural characteristics in various applications.¹ The structural diversity and durability of POMs make them appropriate for a variety of catalytic applications, such as oxidation, acid catalysis, and as promising components in energy storage systems.^{2–4} Their capacity to perform multi-electron redox reactions while maintaining structural integrity is particularly advantageous in catalysis. For instance, POMs have been successfully used in the selective oxidation of alcohols, such as the conversion of benzyl alcohol into benzaldehyde. Benzaldehyde is generated *in situ* and reacts with aniline to form an imine (Schiff base) in a one-pot reaction, which is a crucial process in chemical synthesis. This technique takes

advantage of the high redox potential and acidity of POMs, which enhance the reaction under mild circumstances.

POMs were synthesised by combining inorganic metal oxides of early transition metals in their higher oxidation states, such as tantalum (Ta^V), molybdenum (Mo^{VI}), vanadium (V^V), niobium (Nb^V), and tungsten (W^{VI}).^{5–9} Most notably, the properties of POMs can be altered by modifying their structural dimensions, composition component, and organic bridging element.^{5,10} Because of their unique properties, POMs are used in applications pertaining to radionuclide capture,^{11,12} drug chemistry,^{13–18} material design,^{19,20} sensing detection,^{21–26} electronics,^{27–30} energy storage,^{4,31–37} crystal engineering,^{38,39} catalysis,^{30,40–56} photocatalysis,^{57–63} and electro-catalysis.^{64,65} POMs can be classified into two categories based on their chemical composition: isoPOMs (isopolyoxometalates) and heteroPOMs (heteropolyoxometalates). Common structural motifs for iso- and hetero-polyoxometalates include the Lindqvist anion [Mo₆O₁₉]²⁻ and the Keggin anion [XW₁₂O₄₀]ⁿ⁻.^{66–70} The hexamolybdate, or Lindqvist structure, is a typical isoPOM made solely of molybdenum and oxygen atoms.^{46,71,72} The Keggin structure, however, is a well-known heteroPOM that integrates various metals and heteroatoms, such as silicon or phosphorus, within its tungsten-oxygen framework.

Sardar Vallabhbhai National Institute of Technology, Ichchhanath, Surat-395 007, Gujarat, India. E-mail: ritambhara.jangir@chem.svnit.ac.in

† Electronic supplementary information (ESI) available. CCDC 2361592–2361594 (1–3). For ESI and crystallographic data in CIF or other electronic format see DOI: <https://doi.org/10.1039/d4dt02289k>

Studies have found that the design and synthesis of novel hexamolybdate and octamolybdate structures with unique topologies pose significant challenges in materials chemistry. However, despite these challenges, the pursuit of novel hexamolybdate and octamolybdate structures continues to be a stimulating area of research, driven by the potential to discover new materials with tailored properties and applications. As advances in synthetic methods and characterization techniques progress, we may expect to see more contributions to this field in the future. The presence of simple anions in a solution (usually water) at different pH and temperature levels leads to the formation of all-inorganic POMs. Several POM structures are produced as a result of this process, and the particular environmental circumstances that exist at the time of formation have an impact on them.

In this paper, we develop three types of polyoxometalate-supported transition metal complexes: copper metal DMF complex based on an octamolybdate, $[\text{Cu}(\text{DMF})_4(\text{Mo}_8\text{O}_{26}) \cdot 2\text{C}_3\text{H}_8\text{NO}] \cdot 1.8 \text{ DMF}$ (**1**); cobalt and nickel DMSO complexes supported on a hexamolybdate; $[\text{Co}(\text{DMSO})_6][\text{Mo}_6\text{O}_{19}]$ (**2**); and $[\text{Ni}(\text{DMSO})_6][\text{Mo}_6\text{O}_{19}]$ (**3**). Studies have shown that complexes with variable metals have diverse characteristics. Double complex salts have potential as precursors for self-organized materials by enabling the synthesis of medicines, thermosensitive materials, catalysts, and analytical reagents.^{73,74} The synergistic effect can result in enhanced performance or entirely new functionalities, making bimetallic coordination compounds promising candidates for the development of advanced materials. Overall, the diverse properties and tunable nature of bimetallic coordination compounds make them attractive for designing materials with tailored functionalities, thus opening up avenues for innovation in various industrial applications.^{75,76} From the perspective of molecular design, we have tried to construct such molecular assemblages using straightforward synthesis. One of our intentions in introducing metal ions into the framework designed by polyanions and organic units is to combine polyanions with organic groups through metal ions and gain stable crystals. Another aim is to acquire catalytic activity because polyoxometalate anions are good electron acceptors, while dimethylformamide (DMF) and dimethyl sulfoxide (DMSO) are electron-rich donors capable of electron transfer. These highly polar solvents can solvate a wide range of polar and nonpolar compounds, making them versatile media for various reactions.^{77,78} The incorporation of the $[\text{Cu}(\text{DMF})_4]$ between two octamolybdates results in the transformation of otherwise inactive parent POMs into useful catalysts, which effectively catalyses the oxidative cross-coupling of anilines, benzyl alcohol, and sodium azide. This reaction occurs in the presence of TBHP at moderate temperatures. This scheme is a one-pot process that incorporates several reactions: C–H functionalisation, condensation, *ortho* selective amination, and cyclization. The synthesis of polyoxometalate-complex hybrids is a difficult process, achieving accurate control over their assembly is not always easy. In the present work, polyoxometalate hybrids are synthesized using molybdenum trioxide (MoO_3)

and metal acetate. Instead of using Na_2MoO_4 or $(\text{NH}_4)_6[\text{Mo}_7\text{O}_{24}]$ as the Mo source, MoO_3 is chosen because it does not contain an extra cation that interferes with the complex hybrid's ability to self-assemble or alter its solubility.

Recent improvement in transition-metal-catalysed C–H functionalization procedures employing pointing groups has resulted in the formation of efficient techniques for the selective production of carbon–carbon and carbon–heteroatom bonds.^{79,80} A very effective copper–molybdate (bimetallic catalyst) catalyzed oxidative cross-coupling reaction is developed for the synthesis of functionalized benzimidazoles. This reaction necessitates the use of anilines, primary alkyl amines, and sodium azide and proceeds through a domino transamination, *ortho* selective amination, and cyclization series. The copper catalyst likely plays a crucial role in facilitating the oxidative cross-coupling reaction and promoting the desired transformations. This type of synthetic methodology can be valuable in the fields of organic synthesis, providing a route to diverse and functionalized benzimidazole derivatives, which have various applications in medicinal chemistry and material science. Benzimidazoles are very valuable structural frameworks in the field of medicinal chemistry due to their wide range of significant pharmacological and biological characteristics. The benzimidazole core is present in a diverse array of bioactive chemicals, rendering it a valuable foundational component for the development and production of pharmacological medicines.^{81–83} Benzimidazoles represent privileged structural scaffolds in medicinal chemistry owing to their diverse and interesting medicinal and biological properties.⁸⁴ In the present work, the obtained POM-based hybrids are employed to make benzimidazole and derivatives. It is found that copper-based octamolybdate, $[\text{Cu}(\text{DMF})_4(\text{Mo}_8\text{O}_{26}) \cdot 2\text{C}_3\text{H}_8\text{NO}] \cdot 1.8 \text{ DMF}$ (**1**), exhibits excellent catalytic activities for these oxidative cross-coupling reactions.

2. Experimental sections

2.1. Materials and methods

All raw ingredients were obtained from commercial sources and used as received. Purification techniques for solvents were used, as reported in the literature.⁸⁵ All the beginning components and the final products were determined to be resistant to moisture and air. Hence, no special precautions are required to exclude air completely. The starting materials (*i.e.* molybdenum trioxide (MoO_3), $\text{Cu}(\text{OAc})_2 \cdot \text{H}_2\text{O}$, and $\text{Co}(\text{OAc})_2 \cdot 4\text{H}_2\text{O}$, $\text{Ni}(\text{OAc})_2 \cdot 4\text{H}_2\text{O}$) and solvents, dimethyl formamide (DMF), and DMSO (dimethyl sulphoxide), were bought from Sigma Aldrich and Spectrochem. Infrared spectra (IR) were recorded on a SHIMADZU IR Affinity-1 ATR-FTIR Instrument. Fourier-transform infrared spectroscopy (FTIR) analysis within the wavenumber range of 400–4000 cm^{-1} was performed. ^1H NMR spectra of the catalysis products were recorded on an ECS 400 MHz (JEOL) NMR spectrometer using $\text{DMSO}-d_6$ solvents and tetramethylsilane (TMS) as the external standard. Chemical shifts are provided in parts per million

(ppm). HR-MS spectra were recorded using evo G2-XS QToF 4k (LC MS/MS) with the Acquity H-Class PLUS UPLC System; m/z : 100 000. Elemental analyses of the Cu^(II)-Mo^(VI), Co^(II)-Mo^(VI) and Ni^(II)-Mo^(VI) complexes in percentages of carbon, nitrogen, hydrogen and sulphur were determined using a CHNSO analyser. Thermogravimetric analysis (TGA) was carried out to determine the thermal stability of the complexes in an aluminium pan using a sample weight of 9.00 mg, with a heating rate of 10 °C min⁻¹ in a nitrogen environment (100 mL min⁻¹). Powder X-ray diffraction studies (PXRD) were carried out using an X-ray diffractometer (Panalytical X'Pert Pro) instrument. The data analysis was performed using the Reflex module of Materials Studio V6.0. The catalysis process was monitored using a gas chromatograph (TRACE 1110, Thermo Fisher Scientific India Pvt. Ltd, Navi Mumbai, India), which was equipped with a flame ionization detector.

X-ray single-crystal data collection and refinement. A suitable single crystal of **1–3** with dimensions of 0.23 × 0.21 × 0.16 mm³, 0.271 × 0.217 × 0.211 mm³ and 0.251 × 0.241 × 0.171 mm³ was picked using an optical microscope and sealed to a glass tube. Crystallographic data were collected using a 'Bruker APEX-II CCD' diffractometer with Mo K α radiation at 296.68 K, 296 K and 299.1 K. Using Olex2,⁸⁶ the structure was solved with the ShelXT⁸⁷ structure solution program using intrinsic phasing and refined with the ShelXL⁸⁸ refinement package using least squares minimization. The anisotropic displacement parameters were refined for all non-hydrogen atoms. Hydrogen atoms on ligands are added to the riding model. Crystal data and structural refinements are summarized in Table 1. Selected bond lengths (Å) and angles (°) of **1–3** are listed in ESI.† Crystallographic data for **1–3** are deposited in the Cambridge Crystallographic Data Center with CCDC 2361592–2361594.†

2.2. Synthesis of [Cu(DMF)₄(Mo₈O₂₆)·2C₃H₈NO]·1.8 DMF (1)

A mixture of MoO₃ (3.00 g, 20.83 mmol) with Cu(OAc)₂·H₂O (1.00 g, 5.01 mmol) was added to 50.0 mL of aqueous DMF (H₂O/DMF = 15/35 mL). The solution was stirred at 100 °C for 4 hours after obtaining a clear green solution. Green block crystals appeared after about two days of slow evaporation of solvent at room temperature. Yield: 70%. Anal. cal.: C, 12.63; H, 2.12; N, 4.91. Found as follows: C, 13.33; H, 2.92; N, 5.70. IR (KBr, cm⁻¹): 3482 (br), 3172 (w), 1625 (s), 1525 (m), 1424 (m), 1357 (m), 947 (s), 895 (s), 845 (m), 836 (s), 551 (w).

2.3. Synthesis of [Co(DMSO)₆][Mo₆O₁₉] (2)

A mixture of MoO₃ (3.00 g, 20.83 mmol) with Co(OAc)₂·4H₂O (2.00 g, 0.8029 mmol) was added to 50.0 mL of aqueous DMSO (H₂O/DMSO = 15/35 mL). The solution was stirred at 100 °C for 4 hours after obtaining a clear red solution. Red crystals appeared after about one day of slow evaporation of the solvent at room temperature. Yield: 70%. Anal. cal.: C, 10.24; H, 2.58; S, 13.67. Found as follows: C, 12.71; H, 3.37; S, 14.86. IR (KBr, cm⁻¹): 3404 (br), 3004 (w), 1916 (s), 1661 (s), 1521 (s), 1414 (s), 1311 (m), 1001 (s), 942 (s), 772 (m), 590 (s).

2.4. Synthesis of [Ni(DMSO)₆][Mo₆O₁₉] (3)

A mixture of MoO₃ (3.00 g, 20.83 mmol) with Ni(OAc)₂·4H₂O (0.5 g, 2 mmol) was added to 50.0 mL of aqueous DMSO (H₂O/DMSO = 15/35 mL). The solution was stirred at 100 °C for 4 hours after obtaining a clear yellow solution. Yellow crystals appeared after about one day of slow evaporation of the solvent at room temperature. Yield: 70%. Anal. cal.: C, 10.54; H, 2.72; S, 14.12.

Table 1 Crystallographic data for **1–3**

Parameter	1	2	3
Empirical formula	C ₁₈ CuH ₄₄ Mo ₈ N ₆ O ₃₂	Mo ₆ O ₂₅ C ₁₂ H ₃₆ CoS ₆	Mo ₆ O ₂₅ C ₁₂ H ₃₆ NiS ₆
FW (g mol ⁻¹)	1687.65	1407.34	1407.12
Temperature/K	296.68	296.0	299.1
Crystal system	Triclinic	Triclinic	Triclinic
Space group	<i>P</i> $\bar{1}$	<i>P</i> $\bar{1}$	<i>P</i> $\bar{1}$
<i>a</i> (Å)	11.6217(2)	8.6329(9)	8.64980(10)
<i>b</i> (Å)	11.7346(2)	9.2575(9)	9.2159(3)
<i>c</i> (Å)	11.9051(2)	12.2531(13)	12.2140(4)
α (°)	112.753(2)	94.763(4)	94.803(2)
β (°)	104.637(2)	93.152(4)	93.302(2)
γ (°)	107.424(2)	91.312(4)	91.519(2)
<i>V</i> (Å ³)	1297.20(5)	974.03(17)	968.14(5)
<i>Z</i>	1	1	1
ρ_{calcd} (g cm ⁻³)	2.160	2.399	2.413
μ (mm ⁻¹)	2.357	2.687	2.761
<i>F</i> (000)	815.0	683.0	684.0
Crystal size/mm ³	0.23 × 0.21 × 0.16	0.271 × 0.217 × 0.211	0.251 × 0.241 × 0.171
Radiation	MoK α (λ = 0.71073)	MoK α (λ = 0.71073)	MoK α (λ = 0.71073)
2 θ range for data collection/°	6.85 to 50.7	4.416 to 55.066	4.438 to 53.954
Index ranges	-13 ≤ <i>h</i> ≤ 13, -14 ≤ <i>k</i> ≤ 14, -14 ≤ <i>l</i> ≤ 14	-11 ≤ <i>h</i> ≤ 11, -12 ≤ <i>k</i> ≤ 12, -15 ≤ <i>l</i> ≤ 15	-10 ≤ <i>h</i> ≤ 10, -11 ≤ <i>k</i> ≤ 11, -15 ≤ <i>l</i> ≤ 15
Collected reflections	22 841	35 080	20 208
Independent reflections	4645 [<i>R</i> _{int} = 0.0604, <i>R</i> _{sigma} = 0.0376]	4469 [<i>R</i> _{int} = 0.0515, <i>R</i> _{sigma} = 0.0248]	4044 [<i>R</i> _{int} = 0.0221, <i>R</i> _{sigma} = 0.0165]
Parameters	4645/259/303	4469/0/235	4044/0/235
Goodness-of-fit on <i>F</i> ²	1.062	1.236	1.072
Final <i>R</i> indexes [<i>I</i> ≥ 2 σ (<i>I</i>)]	<i>R</i> ₁ = 0.0439, <i>wR</i> ₂ = 0.1312	<i>R</i> ₁ = 0.0558, <i>wR</i> ₂ = 0.1380	<i>R</i> ₁ = 0.0309, <i>wR</i> ₂ = 0.0685
Final <i>R</i> indexes [all data]	<i>R</i> ₁ = 0.0461, <i>wR</i> ₂ = 0.1330	<i>R</i> ₁ = 0.0578, <i>wR</i> ₂ = 0.1404	<i>R</i> ₁ = 0.0349, <i>wR</i> ₂ = 0.0708

IR (KBr, cm^{-1}): 3482 (br), 3172 (w), 1625 (s), 1525 (m), 1424 (m), 1357 (m), 947 (s), 895 (s), 845 (m), 836 (s), 551 (w).

2.5. Catalysis: oxidation of the cross-coupling of amines and benzyl alcohol

Oxidation of the cross-coupling of amines and alcohol was performed using a screw cap reaction tube. Benzyl alcohol (3 mmol), aniline (1 mmol), sodium azide (2 mmol), AcOH (5 mmol), and TBHP (2.5 mmol) were used as oxidants, and our synthesized three catalysts (10 mol%) were placed in the tube. Optimization of the different reaction solvents for the catalytic oxidation of benzimidazoles with our three synthesized catalysts was performed. A temperature of 80 °C was maintained for six hours. The resulting mixture was subjected to the GC technique to check the completion of the reaction. Further, the resulting mixture was filtered through a Celite pad and washed using ethyl acetate. The filtrate was concentrated under lower atmospheric pressure to remove the ethyl acetate, yielding a concentrated residue. To obtain a pure product, the residue was purified using column chromatography with an eluent mixture of petroleum ether and ethyl acetate.

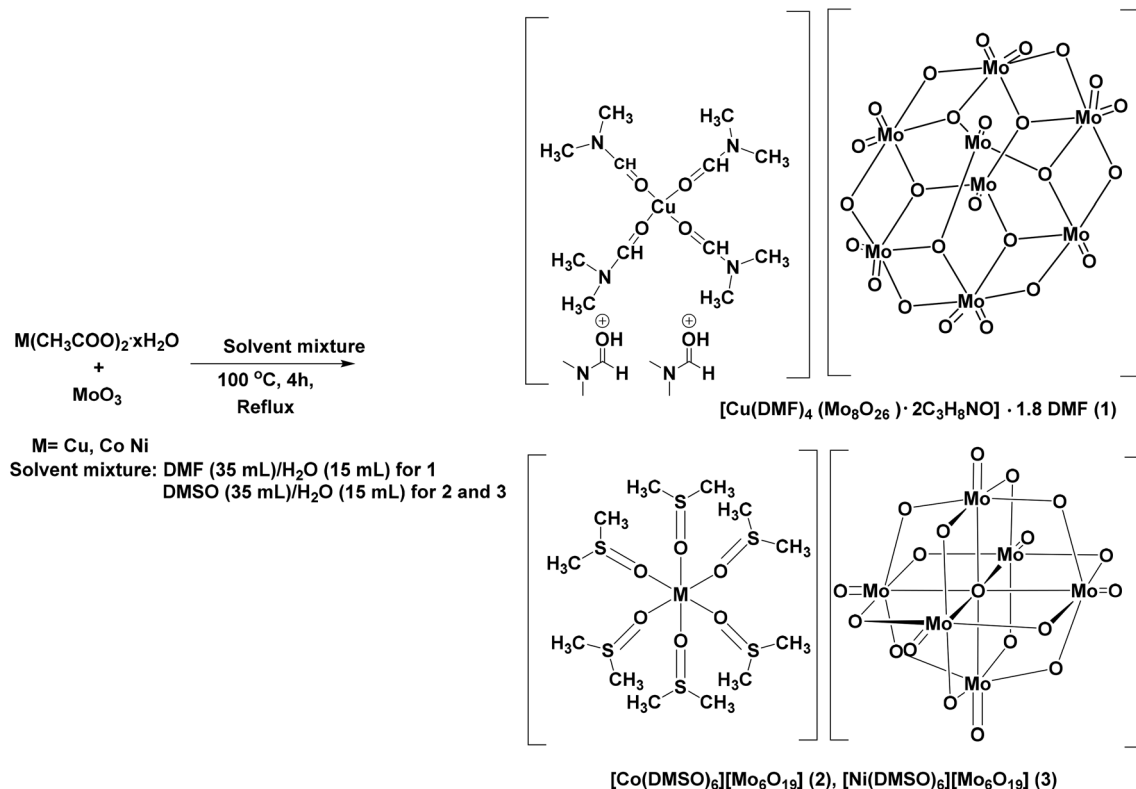
3. Results and discussion

Reactions aiming to prepare compound **1** were first performed under open bench conditions using a mixture of solvents

(DMF/ H_2O). The synthesis involving the mixture of molybdenum trioxide (MoO_3) and $\text{Cu}(\text{OAc})_2 \cdot \text{H}_2\text{O}$ in aqueous DMF solution was stirred at 100 °C (Scheme 1). Green block crystals appeared after two days of slow evaporation of the solvent at room temperature.

The synthesis of compounds **2** and **3** was performed using a DMSO/ H_2O solvent mixture. The mixture of molybdenum trioxide (MoO_3) and metal salts in an aqueous DMSO solution was heated at 100 °C with stirring for 4 hours. Red crystals of compound **2** and yellow block crystals of **3** appeared after about one day of slow evaporation at room temperature. The success of the reaction was first identified by Fourier Transform Infrared Spectroscopy (FT-IR). Two strong absorption bands in **1–3** in the IR spectra in ranges of 795–798 cm^{-1} and 951–954 cm^{-1} are due to $\nu_{(\text{Mo}-\text{O}_{\text{bridged}}-\text{Mo})}$ and $\nu_{(\text{Mo}-\text{O}_{\text{terminal}})}$ stretching vibrations, respectively, which are comparable to similar vibrations in the formerly reported octamolybdate and hexamolybdate complexes (Fig. S1–S3†),^{48,89,90} indicating the structural similarities and characteristic bonding patterns within these polyoxometalates. Medium intensity features in the 780–820 cm^{-1} region are tentatively attributed to $\nu_{(\text{M}-\text{O}-\text{M})}$. The organic region above 1000 cm^{-1} in the spectrum of **1** was dominated by signals of medium-weak intensity associated with C–N bonds that confirmed the presence of the DMF molecule in **1**, and S–O bonds confirmed the presence of DMSO molecules in **2** and **3**.

Thermogravimetric analysis (TGA) studies were conducted under a nitrogen (N_2) gas atmosphere to determine the



Scheme 1 Synthesis of $[\text{Cu}(\text{DMF})_4(\text{Mo}_8\text{O}_{26}) \cdot 2\text{C}_3\text{H}_8\text{NO}] \cdot 1.8 \text{ DMF}$ (**1**), $[\text{Co}(\text{DMSO})_6][\text{Mo}_6\text{O}_{19}]$ (**2**) and $[\text{Ni}(\text{DMSO})_6][\text{Mo}_6\text{O}_{19}]$ (**3**).

thermal stability of the samples over temperatures ranging from ambient temperature to 800 °C. The TGA curve of **1** indicates three distinct phases of weight loss, as shown in Fig. S4.† The first stage, occurring from room temperature to approximately 95–100 °C, shows a weight reduction of 45.55% due to the evaporation of free and loosely bound dimethylformamide (DMF) molecules, corresponding to the loss of around 3.8 DMF molecules. In the second stage, from 100 °C to 230 °C, the Cu(DMF)₄ complex undergoes further decomposition, resulting in a mass reduction of 23.60% as coordinated DMF ligands are eliminated. This stage is marked by the formation of copper oxides, such as CuO or Cu₂O. The final stage, occurring above 300 °C, involves the decomposition of the [Mo₈O₂₆]⁴⁻ polyanion, leading to the formation of smaller molybdenum oxides, such as MoO₃. The TGA curves of compounds **2** and **3** show two distinct phases of weight loss, as shown in Fig. S5 and S6.† The graph of compound **2** indicates three phases of weight loss. The first stage observed in the range of 100–250 °C involves a mass loss of 12.43% primarily due to the evaporation of water molecules and trapped moisture. During this step, six dimethyl sulfoxide (DMSO) ligands, which are weakly coordinated to the cobalt ion, evaporate or decompose, resulting in a significant mass reduction. The second stage in the range of 250–400 °C involves the decomposition of the [Co(DMSO)₆]²⁺ complex, leading to the formation of cobalt oxides (CoO or Co₃O₄) and the release of sulphur dioxide (SO₂), with a 26% mass loss. The final stage in the range of 400–800 °C involves the collapse of the hexamolybdate anion, resulting in the formation of smaller molybdenum oxides, such as MoO₃. The graph of compound **3** reveals a three-stage decomposition process. The first stage, occurring in the range of 85–195 °C, involves the loss of six DMSO ligands and the elimination of water molecules, resulting in a mass loss of 12.78%. The second stage in the range of 190–280 °C shows a further 25% mass loss attributed to the decomposition of the [Ni(DMSO)₆]²⁺ complex, forming nickel oxides (NiO or Ni₃O₄) and releasing sulfur dioxide (SO₂). The

final stage, occurring above 400 °C, involves the collapse of the [Mo₆O₁₉]²⁻ polyanion, leading to the formation of molybdenum oxides, such as MoO₃.

3.1. Single-crystal X-ray diffraction studies

Compound **1** crystallizes in the triclinic space group *P* $\bar{1}$ (Table 1). The molecular structure consists of a cationic copper complex [Cu(DMF)₄]⁴⁺ cation and γ -[Mo₈O₂₆]⁴⁻ anion along with non-bonding DMF molecules in the lattice structure (Fig. 1). The Cu(II) ion exhibits a six-coordinate geometry, forming a distorted octahedral structure. It is coordinated by four DMF molecules *via* the oxygen atoms of the DMF ligands, arranged in a *trans* mode, and two [Mo₈O₂₆]⁴⁻ anion units. The two Cu(II)–octamolybdate bonds are significantly longer (2.394(5) Å) than the Cu(II)–DMF bonds due to the Jahn–Teller effect. Additionally, two DMF molecules, where the nitrogen atoms carry a positive charge, are found in the lattice. Consequently, Cu(II) is in the core, and the remaining two positive charges are balanced by DMF⁺ molecules.

The bond lengths of Cu1–O15, Cu1–O14 and Cu1–O6 are 1.947(5) Å, 1.966(5) Å and 2.394(5) Å, respectively. The bond angles around the Cu atoms are 70.27(16)–162(2)° for O–Mo–O, 86.33(15)–117.3(2)° for Mo–O–Mo, 83.9(2)–180.0(4)° for O–Cu–O, 123.1(5)–123.7(5)° for C–Cu–O, and 120.8(8)–121.7(7)° for C–N–C. Furthermore, the octamolybdate anion [Mo₈O₂₆]⁴⁻ is well identified and compared with α - η isomers.⁴⁸ It is found that octamolybdate exists in its γ form. As shown in Fig. 1, γ -[Mo₈O₂₆]⁴⁻ is composed of eight edge-sharing MoO₆ octahedra, out of which six octahedra are characterized by two terminal oxygen atoms (O_{terminal}) attached to each Mo atom and each of the remaining two Mo octahedra has one O_{terminal}. Overall, the cluster consists of eight μ_2 -oxygen (O_{bridging}) atoms, four μ_3 -oxygen (O_{bridging}) atoms and two μ_4 -oxygen (O_{bridging}) atoms along with the terminal oxygen atoms. All of the Mo–O_{terminal} and Mo–O_{bridging} bond lengths and bond angles are in good accordance with the relevant literature values for reported γ -[Mo₈O₂₆]⁴⁻.^{91,92} The Mo–O bond lengths

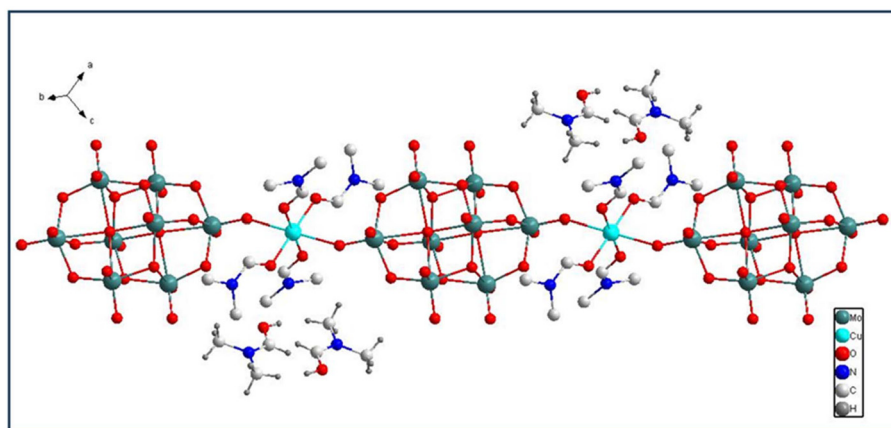


Fig. 1 Ball and stick representation of compound **1**. Cu(DMF)₄ is between two {Mo₈O₂₆]⁴⁻ units and colour code: Mo, green; Cu, cyan; O, red; N, blue; C, grey and H, black.

vary from 1.683(5) to 2.407(4) Å in accordance with those in the previously reported molybdate structures.^{16,26} The bond valence sum (BVS) calculations show that all Mo atoms are in the highest oxidation state (+VI). Along the *a*-axis, the octamolybdate anion $[\text{Mo}_8\text{O}_{26}]^{4-}$ clusters aggregate to form 1D molybdate chains that are parallel to each other *via* numerous Mo–O bonds, and the 1D hybrid complex is constructed by the coordination between Cu(II) and terminal oxygen atoms (O6) from the 1D chains simultaneously (Fig. 2 and 3).

Additionally, Fig. S10† illustrates the hydrogen bonding interactions between the $[\text{Cu}(\text{DMF})_4]$ and non-bonding DMF ligands and oxygen atoms of the γ - $[\text{Mo}_8\text{O}_{26}]^{4-}$ anions. These interactions contribute to the formation of a 2D network (Fig. 3) (Fig. S7b:† 2.854 Å for bond lengths O11...H2C, 2.577 Å for bond lengths O7...H2C, 2.533 Å for bond lengths O7...H3A and 2.681 Å for bond lengths O6...H7B).

Compounds 2 and 3 exhibit a triclinic space group $P\bar{1}$ crystal structure with a 1D arrangement. The metal–organic loops, *i.e.* $[\text{Co}(\text{DMSO})_6]$ and $[\text{Ni}(\text{DMSO})_6]$, are attached in a staggered manner to the anions $[\text{Mo}_6\text{O}_{19}]^{2-}$ (Fig. 4 and 5). This combination provides insights into the spatial arrangement and connectivity of the components within the crystal lattice of these complexes. The valence sum calculations revealed that all molybdenum atoms in compounds 2 and 3 had an oxidation state of +VI. This information is valuable for understanding the electronic structure and bonding in these complexes, especially in the context of the anions $[\text{Mo}_6\text{O}_{19}]^{2-}$. The $[\text{Mo}_6\text{O}_{19}]^{2-}$ is the famous Lindqvist structure, which consists of central oxygen atoms arrayed with six metal atoms in an octahedral geometry. The $[\text{Mo}_6\text{O}_{19}]^{2-}$ shows three kinds of oxygen atoms: terminal oxygen O_t , double bridge oxygen O_b and central oxygen O_c . Compounds 2 and 3 consist of Co^{III}

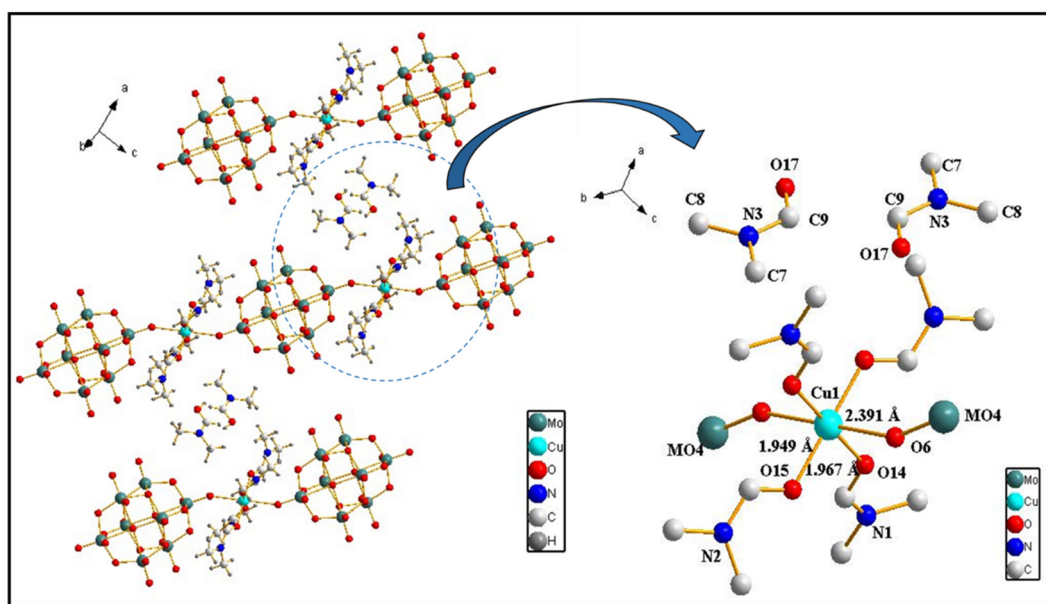


Fig. 2 View of the 2D network constructed by double helical strands extended γ -octamolybdate in 1.

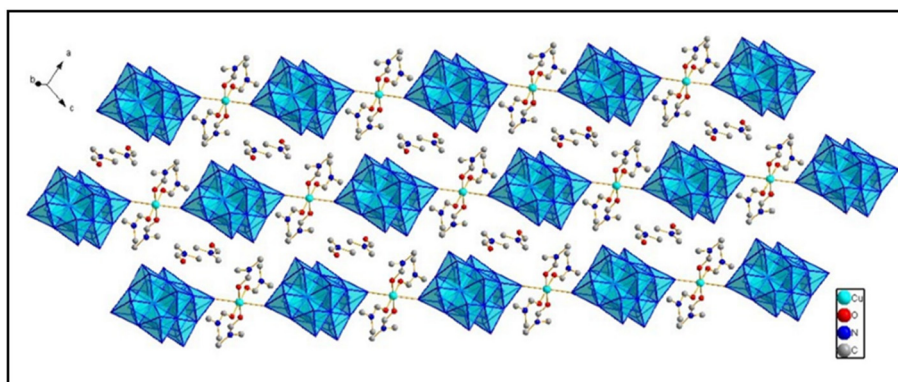


Fig. 3 View of the 2D network constructed by the ball-and-stick representation of $[\text{Cu}(\text{DMF})_4]$ and non-bonded DMF molecules, with the blue-colour polyhedra representation extended by the octamolybdate unit in 1.

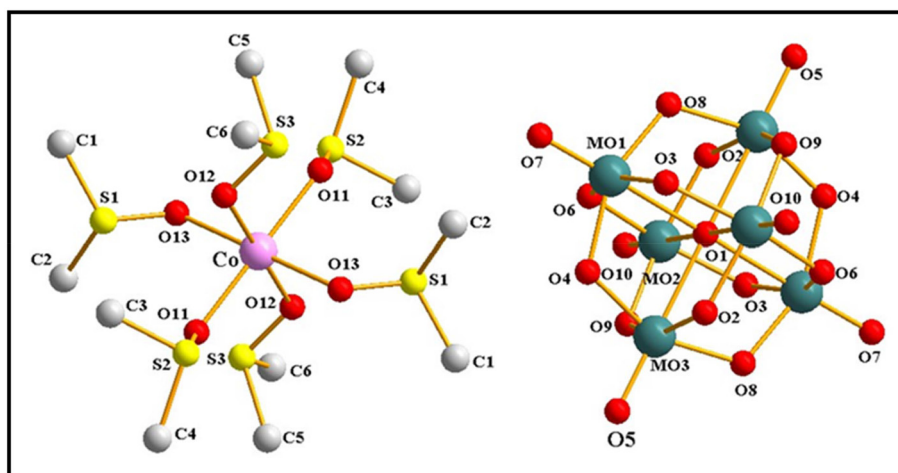


Fig. 4 Ball and stick representation of **2** and colour code: Mo, green; Co, pink; O, red; S, yellow; C, grey. All hydrogen atoms are omitted for clarity.

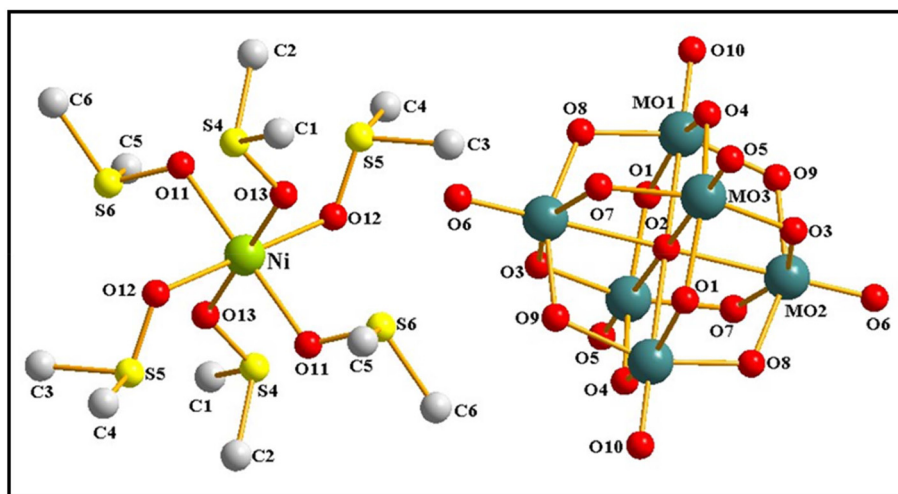


Fig. 5 Ball and stick representation of **3** and colour code: Mo, green; Ni, light green; O, red; S, yellow; C, grey. All hydrogen atoms are omitted for clarity.

and Ni^(II) atoms that create a slightly distorted octahedral configuration by coordinating with DMSO ligands. The slightly distorted octahedral configuration suggests some asymmetry or structural deviations from a perfect octahedron. The use of DMSO as a coordinating ligand indicates the presence of chemical interactions between the metal centers and the surrounding ligands, contributing to the overall structure and stability of the compounds. The cobalt(II) center in **2** has a deformed octahedral-based coordination geometry and is coordinated with six O atoms derived from the six DMSO ligands. Co1–O11, Co1–O12, and Co1–O13 have bond lengths 2.073(3) Å, 2.112(3) Å, and 2.119(3) Å, while S2–O11, S3–O12, and S1–O13 have sulfur–oxygen bond lengths 1.522(3) Å, 1.523(3) Å, and 1.526(3) Å, respectively. Similarly, in **3**, the nickel(II) core exhibits a distorted octahedral coordination geometry formed by the six oxygen atoms of the DMSO ligands. The bond lengths between NiO4–O11, NiO4–O12, and NiO4–O13

are 2.072(2) Å, 2.089(2) Å, and 2.042(2) Å, respectively. The sulfur–oxygen bond lengths between S4–O13, S5–O12, and S6–O11 are 1.516(2) Å, 1.520(2) Å, and 1.521(2) Å, respectively. The bond angles surrounding the cobalt atoms are 75.94(11)–179.9(3)° for O–Mo–O, 89.64(3)–180.0° for Mo–O–Mo, 88.35(13)–180.0° for O–Co–O, 103.9(2)–105.4(3)° for O–S–C, and 98.0(3)–99.4(4)° for C–S–C. Moreover, the bond angles surrounding the nickel atoms are 75.99(9)–179.7(3)° for O–Mo–O, 89.680(19)–180.00(2)° for Mo–O–Mo, 88.92(10)–180.0° for O–Ni–O, 103.61(19)–105.52(19)° for O–S–C, and 98.5(2)–98.8(3) for C–S–C. Additionally, the hydrogen bonding interactions between the [M(DMSO)₆] and oxygen atoms of the [Mo₆O₁₉]²⁻ anions are illustrated in Fig. S8b and S10b.†

The phase identity and purity of **1–3** were confirmed by powder XRD, with patterns matching closely to those from single-crystal XRD (Fig. 6). For compound **1**, PXRD showed sharp peaks in the 2θ range of 5°–10° (at 8.78°, 9.11°, and

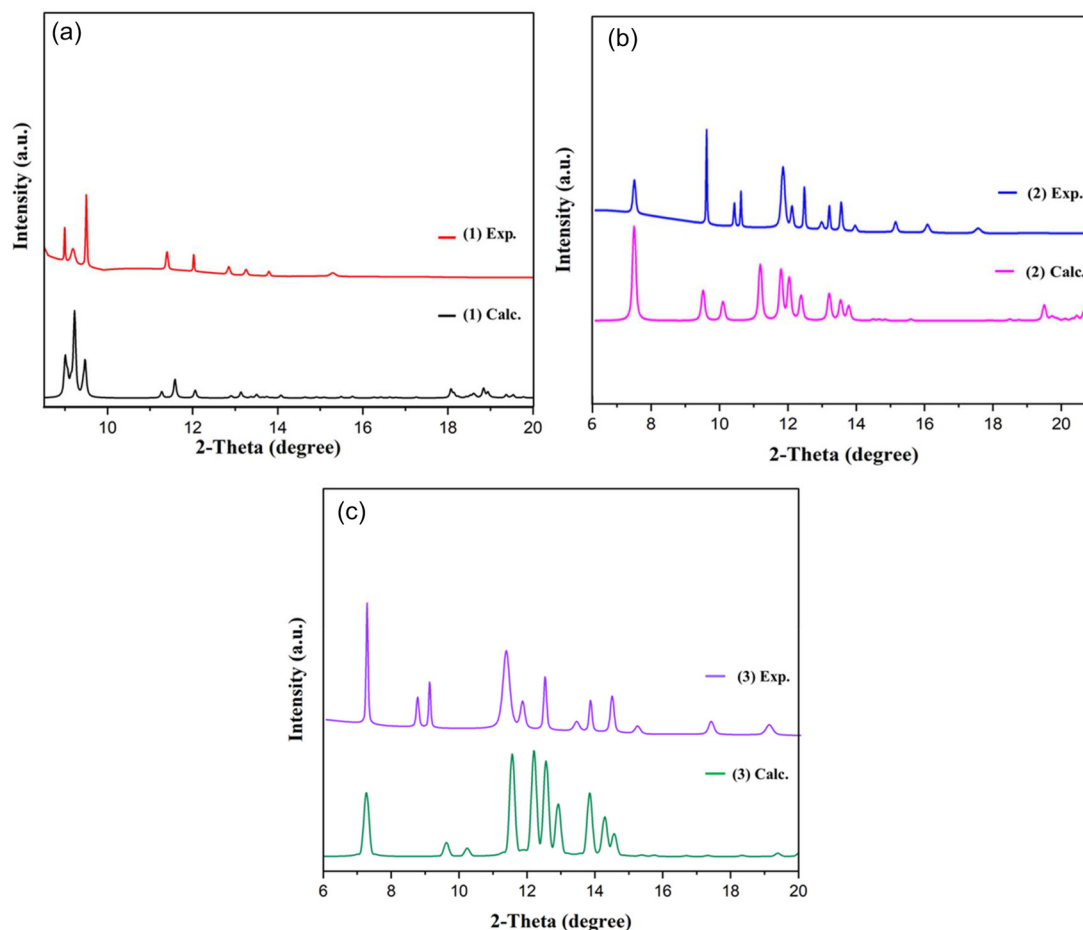


Fig. 6 PXRD patterns (Exp. vs. Calc.) of **1** (a), **2** (b), and **3** (c).

9.51°), corresponding to the (*hkl*) planes (100), (010), and (10 $\bar{1}$). The slight shift of the 8.78° peak to a lower angle suggests lattice expansion due to strain or larger ion incorporation, confirming phase purity. Compound **2** exhibited sharp bands in the 2θ range of 5°–15°, with peaks at 7.23°, 9.59°, 10.27°, 11.51°, 12.22°, 12.48°, 12.90°, 13.85°, 14.27°, and 14.52°, corresponding to the (001), (010), (100), (01 $\bar{1}$), (10 $\bar{1}$), (011), (101), (1 $\bar{1}$ 0), (110), and (002) planes, respectively. Compound **3** showed peaks at 2θ values of 7.27°, 9.63°, 10.23°, 11.56°, 12.21°, 12.57°, 12.92°, 13.85°, 14.28°, and 14.59°, which correspond to the (001), (010), (100), (01 $\bar{1}$), (10 $\bar{1}$), (011), (101)(10), (110) and (002) planes, respectively. The observed diffraction pattern closely matches the simulated pattern derived from single-crystal XRD data, indicating phase purity and consistency in the crystalline structure. This alignment affirms the accuracy of the synthesized compounds, supporting the absence of significant impurities or deviations in lattice parameters.

3.2. Cu^(II)–Mo^(VI) complexes as catalysts

Benzimidazole derivatives are structural bio-isosteres of naturally occurring purine bases, such as adenine and guanine. The benzimidazole nucleus is a heterocyclic aromatic com-

pound containing a fused imidazole ring system. This structural motif has been found in various biologically active molecules, and researchers have explored its potential pharmacological applications. Due to their diverse pharmacological activities, researchers have been interested in developing and studying benzimidazole derivatives for medicinal purposes. The recognition of benzimidazole's biological effects has led to the synthesis and investigation of numerous derivatives to understand their structure–activity relationships and optimize their pharmacological properties for specific therapeutic applications. This research contributes to the development of new pharmaceutical agents with improved efficacy and reduced side effects. The use of Cu^(II)–Mo^(VI) catalyst and TBHP for the selective oxidation of benzyl alcohol to benzaldehyde, followed by an *in situ* reaction with aniline to form imine (Schiff bases), is a robust method in organic synthesis. This approach combines efficiency, high selectivity, and simplicity, making it valuable for various industrial applications. Benzaldehyde, formed *in situ*, reacts with aniline to produce an imine (Schiff base) in a one-pot reaction. This reaction involves the nucleophilic attack of the amine group of aniline on the carbonyl group of benzaldehyde, followed by dehydration to form the Schiff base. This method is advantageous, as it reduces the

number of steps and minimizes the need for intermediate purification.

The selective and efficient oxidation of benzyl alcohol to benzaldehydes using our synthesized catalyst described above encouraged us to continue the reaction towards the one-pot synthesis of benzimidazoles by the addition of aniline (Scheme 2). Optimization of several reaction conditions for the catalytic oxidation of benzimidazoles using $\text{Cu}^{\text{III}}\text{-Mo}^{\text{VI}}$ is performed (Fig. 7). In this procedure, dimethyl sulfoxide (DMSO) is found to be a highly effective solvent.

$\text{Cu}^{\text{III}}\text{-Mo}^{\text{VI}}$ complexes have been extensively studied as catalysts for various organic transformation reactions.^{1,93–96} These complexes often exhibit interesting redox properties, making them intriguing for catalytic applications. The presence of both copper and molybdenum allows for a synergistic effect, enhancing the overall catalytic activity and selectivity. Typically, a great variety of Mo complexes can be used, but further studies have shown that the nature of the ligands around the molybdenum center is critical to the success of the reaction. However, varying the nature of the copper(II) counterion has effects on the rate/yield of the reaction. The synergistic effect of copper and molybdenum improves the overall catalytic activity. Our catalyst is highly selective (selectivity: >99%) and efficient (conversion: >99%) for the oxidation cross-coupling of anilines, benzyl alcohol, and sodium azide. At a moderate temperature, this reaction occurs in the presence of TBHP. This method is a one-pot synthesis of the benzimidazole procedure that incorporates a sequence of reactions. The substrate scope was assessed using benzyl alcohol derivatives (with H, Me, and Cl substituents) once the appropriate reaction conditions were determined (Table 2).

The catalytic potential of some Mo-containing materials ($\text{Na}_2\text{MoO}_4 \cdot 2\text{H}_2\text{O}$, $(\text{NH}_4)_4[\text{Mo}_8\text{O}_{26}] \cdot 4\text{H}_2\text{O}$, and $(^t\text{Bu}_4\text{N})_4[\text{Mo}_8\text{O}_{26}]$) was also assessed to compare with $\text{Cu}^{\text{III}}\text{-Mo}^{\text{VI}}$ complex (Fig. 8). When substituting the $\text{Cu}^{\text{III}}\text{-Mo}^{\text{VI}}$ catalyst by applying the above-mentioned materials, the benzyl alcohol % conversion and % yield of 2-phenylbenzimidazole decrease to 50–80% and 5–10%, respectively. Benzyl alcohol with aniline using TBHP as the oxidant to form 2-phenyl benzimidazole in the presence of $\text{Cu}(\text{OAc})_2$ in DMSO yields only 45% of the product.⁹⁷ Our catalytic reaction is better due to the economical and ease of productivity of the catalyst, especially when compared to previously reported catalytic reactions, which required exorbitant catalysts involving nanocatalyst ($\gamma\text{-Fe}_2\text{O}_3 @ \text{SiO}_2 / \text{VB1} / \alpha\text{-Mo}_8\text{O}_{26} = \text{SMNPB1Mo}$) that requires a longer duration for the reaction of styrene and *o*-phenylene-

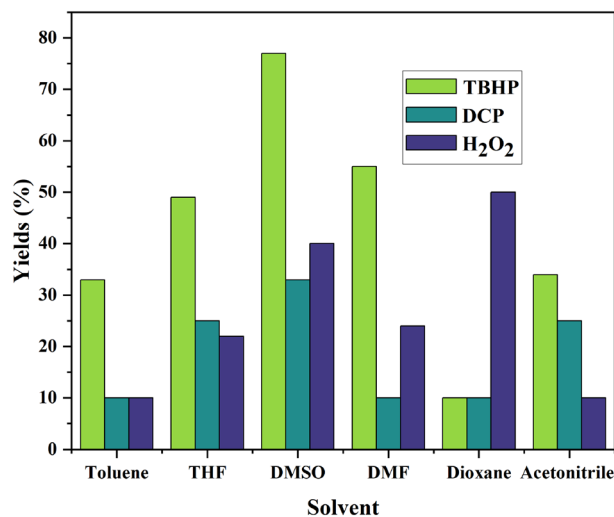
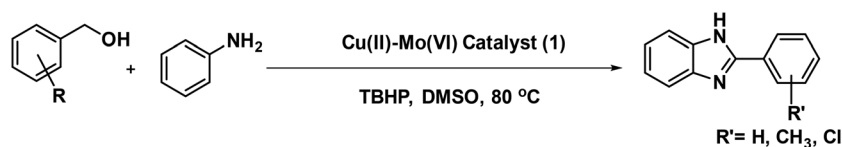


Fig. 7 Optimization of the different reaction conditions for the catalytic oxidation of benzimidazoles with $\text{Cu}^{\text{III}}\text{-Mo}^{\text{VI}}$ (1).

diamine.⁹⁸ The Ag₃PMo catalyst was used for benzene-1,2-diamine and benzaldehyde,³⁰ and $\text{Fe}_3\text{O}_4 @ \text{Sal} @ \text{Cu}$ catalyst was employed for a mixture of benzaldehyde derivatives and *o*-phenylenediamine derivatives under ultrasonic irradiation to synthesize 2-phenyl-1*H*-benzo[*d*]imidazole.⁹⁹ Our catalyst, $\text{Cu}^{\text{III}}\text{-Mo}^{\text{VI}}$, demonstrates superior performance under optimized conditions, highlighting its potential for efficient and selective oxidative cross-coupling reactions, which provide excellent to good yields.

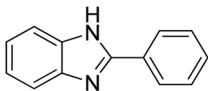
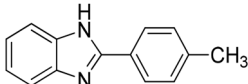
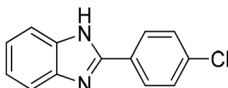
It is found that benzyl alcohols with bromo and chloro functionalities yielded moderate amounts (45% yield) of benzimidazoles in the oxidative cross-coupling reactions using TBHP and $\text{Cu}(\text{OAc})_2$ (80 °C for 12 hours) in acetic acid.⁹⁷ When compared to this homogeneous system, the benefit of our heterogeneous catalytic system is that the oxidation of benzyl alcohol occurs in tandem with aniline to benzimidazole.⁹⁷ The heterogeneous magnetic catalyst system has lower toxicity and is easier to recover from the reaction mixture. Additionally, for the $\text{Cu}^{\text{III}}\text{-Mo}^{\text{VI}}$ complex, the yields are noticeably greater at moderate temperatures with faster reaction times.

A plausible mechanism for the catalytic reaction is given based on previous reports.⁹⁷ The reaction involves the oxidative coupling of benzyl alcohol to benzaldehyde, facilitated by $\text{Cu}^{\text{III}}\text{-Mo}^{\text{VI}}$ catalytic centers. The key steps of the mechanism are summarized below:



Scheme 2 Selective oxidation of benzyl alcohol to benzaldehydes catalyzed by $\text{Cu}^{\text{III}}\text{-Mo}^{\text{VI}}$ (1) for the one-pot tandem synthesis of benzimidazoles.

Table 2 Catalytic oxidation reaction of aniline with different benzyl alcohol substrates

Entry	Product	Conversion (%)	Selectivity (%)	Yields (%)
1		>99	>99	90%
2		>99	>99	80%
3		>99	>99	86%

Reaction conditions: aniline (1 mmol), benzyl alcohol (3 mmol), Cu^(II)-Mo^(VI) catalyst (10 mol%), NaN₃ (2 mmol), TBHP (2.5 mmol), AcOH (5 mmol), DMSO (4 mL), 80 °C, 6 hours used. Products were confirmed using ¹H NMR, IR and mass spectrometry.

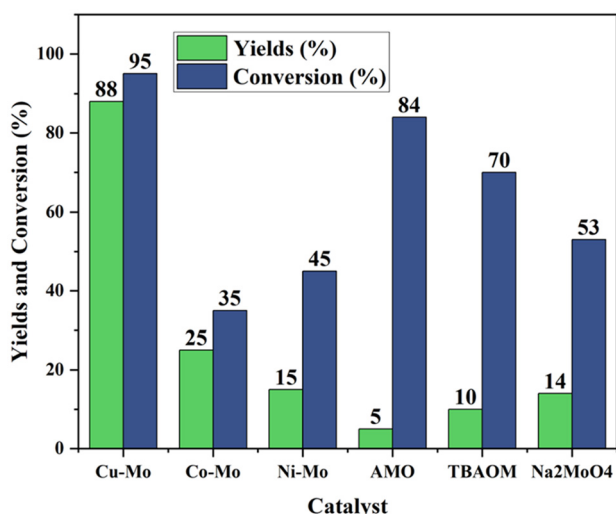


Fig. 8 Catalytic activity of various reported materials for the conversion of benzyl alcohol and aniline into 2-phenylbenzimidazole. TBAOM: (tⁿBu₄N)₄[Mo₈O₂₆], AOM: (NH₄)₆Mo₇O₂₄·4H₂O, Na₂MoO₄. In this work, Cu-Mo: copper-molybdate (1), Co-Mo: cobalt-molybdate (2), and Ni-Mo: nickel-molybdate (3).

Step 1: Generation of radicals: ^tBuOO[•] radicals are produced *via* electron transfer from ^tBuOOH (*tert*-butyl hydroperoxide) to the Cu^(II)-Mo^(VI) catalytic centers. These radicals facilitate the oxidation of benzyl alcohol (**I**) to benzaldehyde (**II**).

Step 2: Condensation: benzaldehyde undergoes condensation with aniline (**III**), leading to the formation of an intermediate imine or Schiff base (**IV**).

Step 3: Coordination and intermediate formation: coordination of intermediate (**IV**) with Cu^(II)-Mo^(VI) produces another intermediate (**V**). **V** reacts with *in situ* produced N₃ radicals from HN₃ and TBHP to generate an intermediate (**VI**). Acetic acid is used to generate hydrogen azide (HN₃) from sodium azide (NaN₃). The *in situ*-generated HN₃ subsequently participates in the reaction by forming N₃ radicals, which are critical for the progression of the catalytic cycle, including the formation of key intermediates and the final cyclization process.

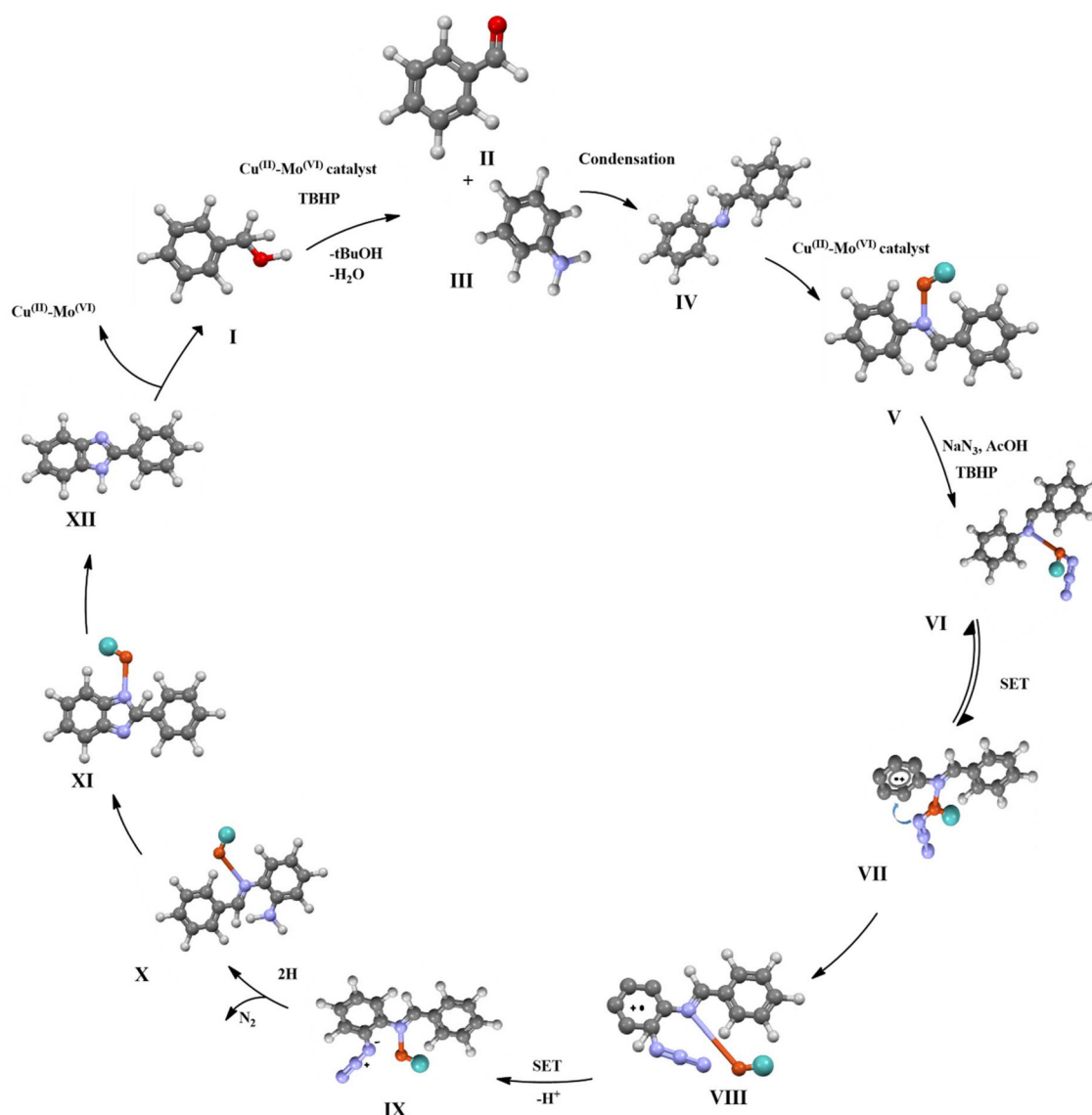
Step 4: Single Electron Transfer (SET) and azido transfer: **VII** is formed through SET from the aryl ring to the metal core. **VII** converts to **VIII** by azido transfer into the aryl ring.

Step 5: SET process and cyclization: **VIII** undergoes another SET process to form **IX**. Upon heating in the presence of Cu^(II)-Mo^(VI), **IX** transforms to **X**.

Step 6: Intramolecular oxidative cyclization: **X** undergoes intramolecular oxidative cyclization to produce **XI**. **XI** aromatizes to form **XII**, completing the catalytic cycle (Scheme 3).

3.3. Reusability and stability of the catalyst

The reusability and stability of a catalyst are key determinants of its practicality for large-scale applications, influencing the economic, environmental, and operational aspects of industrial processes. Researchers and industries continually strive to develop catalysts with enhanced longevity and performance to meet the demands of sustainable and efficient large-scale production. After achieving catalytic conversion to 2-phenylbenzimidazole (Table 2, product 1), the reaction mixture was treated with ethyl acetate. The catalyst was then separated using centrifugation. Centrifugation helps in separating the solid material from the reaction mixture, while ethanol washing may help in removing any residues or by-products formed during the catalytic reaction. The recovered catalyst was subjected to vacuum drying to remove any remaining solvent molecules and ensure thorough drying of the material. The dried catalyst was reused in subsequent reactions to test its reusability and stability. The efficiency of the catalyst was assessed over multiple cycles. The results indicated that the catalyst retained a significant portion of its activity even after several runs, with only a minimal loss in product yield, showing that the catalyst retained its efficiency (Fig. S21, ESI†). This demonstrates the catalyst's robustness and potential for practical applications. To further investigate the catalyst's behaviour, a hot filtration test was performed. After 3 hours of reaction, the catalyst was quickly removed using centrifugation, and the filtrate was allowed to continue stirring at 80 °C for an additional 3 hours. The results revealed that essentially no further reaction happened when the catalyst was



Scheme 3 Proposed reaction pathway of oxidation of benzyl alcohol to benzaldehydes catalyzed by $\text{Cu}^{\text{III}}\text{-Mo}^{\text{VI}}$ complex for the one-pot tandem synthesis of benzimidazoles.

removed, implying that the catalytic activity was mostly due to the solid catalyst rather than any leached species. Furthermore, an ICP-OES analysis was performed to evaluate the metal content of the catalyst. The analysis revealed that the molybdenum and copper percentages in the catalyst used after five runs were 1.85% and 1.77%, respectively, compared to 2% and 1.95% for the fresh catalyst. This corresponds to a Mo and Cu loss of only 7.5% and 9.2%, respectively, in line with the results from the hot filtration test, confirming that the catalyst predominantly acts as a heterogeneous catalyst with minimal leaching. Five consecutive catalytic runs were conducted to assess the catalytic activity of the $\text{Cu}^{\text{III}}\text{-Mo}^{\text{VI}}$ (1). Each catalytic run likely involved exposing the material to specific reactants to observe its catalytic performance. Furthermore, following each reaction cycle, the FT-IR spectra (Fig. S23, ESI[†]) and PXRD patterns (Fig. S24, ESI[†]) of the catalysts were monitored.

This analysis provides additional evidence of the structural integrity and the reactivity of the catalysts throughout the reaction process.

4. Conclusion

In this work, we present the synthesis and X-ray single-crystal structure analyses of three polyoxometalate-supported transition metal complexes: copper-supported octamolybdate, $[\text{Cu}(\text{DMF})_4(\text{Mo}_8\text{O}_{26})\cdot 2\text{C}_3\text{H}_8\text{NO}]\cdot 1.8\text{DMF}$ (1); cobalt and nickel-supported hexamolybdates, $[\text{Co}(\text{DMSO})_6][\text{Mo}_6\text{O}_{19}]$ (2); and $[\text{Ni}(\text{DMSO})_6][\text{Mo}_6\text{O}_{19}]$ (3). Importantly, the obtained POM-based copper complex exhibits excellent catalytic activities for the oxidation of the cross-coupling of anilines, benzyl alcohol, and sodium azide to make benzimidazole because they are extre-

mely helpful in their extensive range of therapeutic applications and biological functions. Among all the complexes, copper–molybdate ($\text{Cu}^{\text{II}}\text{-Mo}^{\text{VI}}$) is found to be an effective catalyst used in the synthesis of benzimidazole, achieving high yields (80–90%) with reusability, and operational simplicity. The redox behaviour and ability to create an optimal reaction environment contribute to high product yields. Benzimidazoles are also important heterocyclic compounds found in many biologically active molecules, including pharmaceuticals and agrochemicals. The ability to efficiently synthesize benzimidazoles through this catalytic method can streamline their production and potentially lead to the development of new drugs or materials. The combinations of POM hybrids and substrates are nearly limitless; a thorough understanding of the performance and limitations of each component, as well as the ability to link these components in a controlled manner, can serve as a foundation for future development in these disciplines. Investigations are occurring on additional materials in our laboratory that can be used with POMs to further widen the field.

Author contributions

A. P. has done all the experimental studied and designed the entire draft, M. A. D. has supported in the GC analysis, R. J. mentored the entire work and given approval for final version of the manuscript.

Data availability

The data supporting this article are included in the ESI.†

Crystallographic data for 1–3 are deposited at the CCDC under 2361592–2361594.†

Conflicts of interest

There are no conflicts to declare.

Acknowledgements

R. J. and A. P. thank Gujarat Council on Science & Technology (project no. GUJCOST/STI/2021-22/3877) for providing financial support. The single crystal X-ray diffraction data have been collected by Mr Mahesh Shrichand Rathod from School of Chemistry, University of Hyderabad, for which the authors are grateful.

References

- M. Amini, A. Yousofvand, M. Hosseinifard, A. Bayrami and J. Janczak, *Sci. Rep.*, 2024, **14**, 653.
- A.-J. Li, S.-L. Huang and G.-Y. Yang, *Dalton Trans.*, 2023, **52**, 18133–18136.
- M. R. Horn, A. Singh, S. Alomari, S. Goberna-Ferrón, R. Benages-Vilau, N. Chodankar, N. Motta, K. Ostrikov, J. MacLeod, P. Sonar, P. Gomez-Romero and D. Dubal, *Energy Environ. Sci.*, 2021, **14**, 1652–1700.
- Y. Zhang, Y. Li, H. Guo, Y. Guo and R. Song, *Mater. Chem. Front.*, 2024, **8**, 732–768.
- Y. Gao, M. Choudhari, G. K. Such and C. Ritchie, *Chem. Sci.*, 2022, **13**, 2510–2527.
- H. Wu, H.-K. Yang and W. Wang, *New J. Chem.*, 2016, **40**, 886–897.
- Y. Gao, M. Choudhari, G. K. Such and C. Ritchie, *Chem. Sci.*, 2022, **13**, 2510–2527.
- H. Wu, H.-K. Yang and W. Wang, *New J. Chem.*, 2016, **40**, 886–897.
- A. Pardiwala, S. Kumar and R. Jangir, *Dalton Trans.*, 2022, **51**, 4945–4975.
- J. M. Cameron, G. Guillemot, T. Galambos, S. S. Amin, E. Hampson, K. Mall Haidaraly, G. N. Newton and G. Izzet, *Chem. Soc. Rev.*, 2022, **51**, 293–328.
- B. S. Nugroho, M. N. K. Wihadi, F. Grote, S. Eigler and S. Nakashima, *Indones. J. Chem.*, 2021, **21**, 776–786.
- H. Zhang, A. Li, K. Li, Z. Wang, X. Xu, Y. Wang, M. V. Sheridan, H.-S. Hu, C. Xu, E. V. Alekseev, Z. Zhang, P. Yan, K. Cao, Z. Chai, T. E. Albrecht-Schönzart and S. Wang, *Nature*, 2023, **616**, 482–487.
- M. Aureliano, A. Serrano, J. Martins, L. Faleiro, C. Fonseca, G. Fraqueza and R. Lagoa, *Polyoxometalates*, Jenny Stanford Publishing, 2022, pp. 309–358.
- A. Joshi, R. Gupta, B. Singh, D. Sharma and M. Singh, *Dalton Trans.*, 2020, **49**, 7069–7077.
- A. Joshi, S. Acharya, N. Devi, R. Gupta, D. Sharma and M. Singh, *Nanoscale Adv.*, 2023, **5**, 6045–6052.
- A. Joshi, R. Gupta, K. Vaghasiya, R. K. Verma, D. Sharma and M. Singh, *ACS Appl. Bio Mater.*, 2020, **3**, 4025–4035.
- A. Joshi, R. Gupta, D. Sharma and M. Singh, *Dalton Trans.*, 2021, **50**, 1253–1260.
- I. Nowak, A. Issayeva, M. Dąbrowska, A. Wawrzyńczak, H. Jeleń, B. Łęska, A. Abubakirova and A. Tleukeyeva, *Molecules*, 2022, **27**, 5122.
- J.-H. Kruse, M. Langer, I. Romanenko, I. Trentin, D. Hernández-Castillo, L. González, F. H. Schacher and C. Streb, *Adv. Funct. Mater.*, 2022, **32**, 2208428.
- Q. Wang, J. Wang, D. Zhang, Y. Chen, J. Wang and X. Wang, *Polyoxometalates*, 2024, **3**, 1.
- P. Song and T. Wang, *ACS Sens.*, 2022, **7**, 3634–3643.
- L. Chen, J. Geng, Z. Guo and X.-J. Huang, *TrAC, Trends Anal. Chem.*, 2023, **167**, 117233.
- X. Xin, N. Hu, Y. Ma, Y. Wang, L. Hou, H. Zhang and Z. Han, *Dalton Trans.*, 2020, **49**, 4570–4577.
- Y. Hou, D. Chai, B. Li, H. Pang, H. Ma, X. Wang and L. Tan, *ACS Appl. Mater. Interfaces*, 2019, **11**, 20845–20853.
- W. An, X. Zhang, J. Niu, Y. Ma and Z. Han, *Chin. Chem. Lett.*, 2022, **33**, 4400–4404.

- 26 H. Song, M.-S. Guo, J.-F. Wang, Y.-Q. Liu, H.-X. Bi, J. Du, W.-T. An, Y.-Y. Ma and Z.-G. Han, *Polyoxometalates*, 2024, **3**(4), 9140065.
- 27 A. Kondinski and M. Ghorbani-Asl, *Nanoscale Adv.*, 2021, **3**, 5663–5675.
- 28 Y. Hu, Y. Wang, J. Zhao and L. Chen, *Coord. Chem. Rev.*, 2024, **506**, 215724.
- 29 S.-M. Wang, Y.-H. Jin, L. Zhou, K.-H. Wang, H. J. Kim, L. Liu, E. Kim and Z. Han, *ACS Appl. Mater. Interfaces*, 2023, **15**, 56242–56252.
- 30 Y.-F. Liu, X.-L. Lin, B.-M. Ming, Q.-L. Hu, H.-Q. Liu, X.-J. Chen, Y.-H. Liu and G.-P. Yang, *Inorg. Chem.*, 2024, **63**, 5681–5688.
- 31 K. S. Morla, D. Thakre, T. B. Deshmukh, S. Malo, S. Ahamed, R. K. Aparna, S. Sahoo, D. Sarma, K. C. Mondal, B. R. Sankapal and A. Banerjee, *J. Mater. Chem. A*, 2024, **12**, 22013–22029.
- 32 E. Svensson Grape, J. Huang, D. Roychowdhury, T. T. Debela, H. Chang, A. Jenkins, A. M. Schimpf, C. H. Hendon and C. K. Brozek, *ACS Appl. Energy Mater.*, 2024, **7**, 2072–2578.
- 33 D.-H. Guan, X.-X. Wang, L.-N. Song, C.-L. Miao, J.-Y. Li, X.-Y. Yuan, X.-Y. Ma and J.-J. Xu, *Angew. Chem., Int. Ed.*, 2024, **63**, e202317949.
- 34 Y. Hou, P. Han, H. Li, S. Zhang, M. Qin, N. Zhang, B. Fu, R. Mao and S. Ge, *Dalton Trans.*, 2024, **53**, 1541–1550.
- 35 J. Chen, J. Wu, G. Zhuang, B. Li and J. Li, *Inorg. Chem.*, 2022, **61**, 10263–10266.
- 36 L. Ni, G. Yang, Y. Liu, Z. Wu, Z. Ma, C. Shen, Z. Lv, Q. Wang, X. Gong, J. Xie, G. Diao and Y. Wei, *ACS Nano*, 2021, **15**, 12222–12236.
- 37 L. Ni, J. Gu, X. Jiang, H. Xu, Z. Wu, Y. Wu, Y. Liu, J. Xie, Y. Wei and G. Diao, *Angew. Chem.*, 2023, **135**, e202306528.
- 38 S. Roy, D. Mumaraddi, A. Jain, S. J. George and S. C. Peter, *Inorg. Chem.*, 2018, **57**, 590–601.
- 39 N. Ogiwara, M. Tomoda, S. Miyazaki, Z. Weng, H. Takatsu, H. Kageyama, T. Misawa, T. Ito and S. Uchida, *Nanoscale*, 2021, **13**, 8049–8057.
- 40 S.-M. Zhang, Y. Wang, Y.-Y. Ma, Z.-B. Li, J. Du and Z.-G. Han, *Inorg. Chem.*, 2022, **61**, 20596–20607.
- 41 M. Guillen-Soler, N. V. Vassilyeva, E. P. Quirós-Díez, J. M. Vila-Fungueiriño, A. Forment-Aliaga and M. d. C. Gimenez-Lopez, *Adv. Sustainable Syst.*, 2024, **8**, 2300607.
- 42 M. Samaniyan, M. Mirzaei, R. Khajavian, H. Eshtiagh-Hosseini and C. Streb, *ACS Catal.*, 2019, **9**, 10174–10191.
- 43 Y. Wang, Z.-X. Liu, X.-P. Zhao, Y.-Y. Ma, S.-M. Zhang, W.-J. Cui, J. Du and Z.-G. Han, *Chin. J. Struct. Chem.*, 2023, **42**, 100011.
- 44 W. Qu, P. Wei, J. Li, L. Liang, L. Ma and G. Li, *Dalton Trans.*, 2024, **53**, 12610–12619.
- 45 J. Li, J. Ma, C. Wei, Z. Zheng, Y. Han, H. Wang, X. Wang and C. Hu, *Dalton Trans.*, 2024, **53**, 4492–4500.
- 46 Q.-L. Hu, Y.-F. Liu, X.-L. Lin, Z.-F. Lin, J.-W. Cao and G.-P. Yang, *Inorg. Chem.*, 2024, **63**, 8919–8924.
- 47 H. Tian, Y. Pan, N. Xu, J. Miao and Z. Zheng, *Inorg. Chem.*, 2023, **62**, 20228–20235.
- 48 S. Han, Y. Cheng, S. Liu, C. Tao, A. Wang, W. Wei, H. Yu and Y. Wei, *Angew. Chem., Int. Ed.*, 2021, **60**, 6382–6385.
- 49 M. Zhang, Y. Zhai, S. Ru, D. Zang, S. Han, H. Yu and Y. Wei, *Chem. Commun.*, 2018, **54**, 10164–10167.
- 50 Z. Wei, S. Ru, Q. Zhao, H. Yu, G. Zhang and Y. Wei, *Green Chem.*, 2019, **21**, 4069–4075.
- 51 Z. Wu, Y. Zhai, W. Zhao, Z. Wei, H. Yu, S. Han and Y. Wei, *Green Chem.*, 2020, **22**, 737–741.
- 52 G. Dai, Q. Li, D. Zang and Y. Wei, *Green Chem.*, 2023, **25**, 6263–6269.
- 53 K. Li, Y. Liu, G. Yang, Z. Zheng, X. Lin, Z. Zhang, S. Li, Y. Liu and Y. Wei, *Green Chem.*, 2024, **26**, 6454–6460.
- 54 J. Wang, H. Yu, Z. Wei, Q. Li, W. Xuan and Y. Wei, *Research*, 2020, **2020**, 3875920.
- 55 S. Wu, C. Zhao, Y. Dong and L. Yan, *Polyoxometalates*, 2024, **3**, 9140070.
- 56 S. Li, Y. Zheng, G.-C. Liu, X.-H. Li, Z. Zhang and X.-L. Wang, *Polyoxometalates*, 2024, **3**(3), 9140061.
- 57 H.-X. Bi, X.-Y. Yin, J.-Y. He, H. Song, S.-J. Lu, Y.-Y. Ma and Z.-G. Han, *Rare Met.*, 2023, **42**, 3638–3650.
- 58 X.-Y. Yin, H.-X. Bi, H. Song, J.-Y. He, Y.-Y. Ma, T.-T. Fang and Z.-G. Han, *Polyoxometalates*, 2023, **2**, 9140027.
- 59 P.-Y. Zhang, C. Lian, Z.-W. Wang, J. Chen, H. Lv and G.-Y. Yang, *Dalton Trans.*, 2024, **53**, 13409–13415.
- 60 X.-L. Chen, J. Wu, J.-L. Wang, X.-M. Liu, H. Mei and Y. Xu, *Dalton Trans.*, 2024, **53**, 12943–12950.
- 61 Y. Dong, Y. Feng, Z. Li, H. Zhou, H. Lv and G.-Y. Yang, *ACS Catal.*, 2023, **13**, 14346–14355.
- 62 Y.-J. Dong, Z.-M. Su and W. Guan, *Polyoxometalates*, 2024, **3**(4), 9140068.
- 63 F. Wang, C. Jing, J. Ping, D. He, W. Shang, M. Zeng, N. Wang and Z. Jia, *Polyoxometalates*, 2024, **3**, 9140067.
- 64 G. Liu, Y. Chen, Y. Chen, Y. Shi, M. Zhang, G. Shen, P. Qi, J. Li, D. Ma, F. Yu and X. Huang, *Adv. Mater.*, 2023, **35**, 2304716.
- 65 J. Gautam, Y. Liu, J. Gu, Z. Ma, J. Zha, B. Dahal, L.-N. Zhang, A. N. Chishti, L. Ni, G. Diao and Y. Wei, *Adv. Funct. Mater.*, 2021, **31**, 2106147.
- 66 M. M. Heravi and M. Mirzaei, *Polyoxometalate-Based Hybrids and Their Applications*, Elsevier, 2023.
- 67 R. Sheng, R. Sun, L. Chen, R. Lv, Y. Li, T. Du, Y. Zhang and Y. Qi, *Crit. Rev. Anal. Chem.*, 2024, **54**, 315–332.
- 68 L. Yang, Z. Yuan, L. He, L. Han, B. Li and Y. Xu, *Inorg. Chem.*, 2024, **63**, 12564–12571.
- 69 X. Wang, Z. Zhang, Z. Liang and H. Yao, *Adv. Sci.*, 2024, **11**, 2403379.
- 70 Z. Wei, Y. Chang, H. Yu, S. Han and Y. Wei, *Acta Chim. Sin.*, 2020, **78**, 725.
- 71 Y. Xia, Y. Wei, Y. Wang and H. Guo, *Inorg. Chem.*, 2005, **44**, 9823–9828.
- 72 J. Luo, K. Chen, P. Yin, T. Li, G. Wan, J. Zhang, S. Ye, X. Bi, Y. Pang and Y. J. A. C. Wei, *Angew. Chem.*, 2018, **130**, 4131–4136.

- 73 Z. Zhou, S. Zhou, X. Zhang, S. Zeng, Y. Xu, W. Nie, Y. Zhou, T. Xu and P. Chen, *Bioconjugate Chem.*, 2023, **34**, 302–325.
- 74 P. Smirnov, E. Filatov, N. Kuratieva, P. Plyusnin and S. Korenev, *Int. J. Mol. Sci.*, 2023, **24**, 12279.
- 75 Y. Sun, J. Ma, F. Ahmad, Y. Xiao, J. Guan, T. Shu and X. Zhang, *Biosensors*, 2024, **14**, 117.
- 76 K. Loza, M. Heggen and M. Epple, *Adv. Funct. Mater.*, 2020, **30**, 1909260.
- 77 H. Lu, Z. Tong, L. Peng, Z. Wang, S.-F. Yin, N. Kambe and R. Qiu, *Top. Curr. Chem.*, 2022, **380**, 55.
- 78 M. M. Heravi, M. Ghavidel and L. Mohammadkhani, *RSC Adv.*, 2018, **8**, 27832–27862.
- 79 B. Li, A. I. M. Ali and H. Ge, *Chem*, 2020, **6**, 2591–2657.
- 80 M. I. Lapuh, S. Mazeh and T. Besset, *ACS Catal.*, 2020, **10**, 12898–12919.
- 81 O. Ebenezer, F. Oyetunde-Joshua, O. D. Omotoso and M. Shapi, *Results Chem.*, 2023, **5**, 100925.
- 82 Y. T. Lee, Y. J. Tan and C. E. Oon, *Acta Pharm. Sin. B*, 2023, **13**, 478–497.
- 83 Y. T. Lee, Y. J. Tan and C. E. Oon, *Acta Pharm. Sin. B*, 2023, **13**, 478–497.
- 84 H. Kashif and Y. Mohammad Shahar, in *Benzimidazole*, ed. K. Pravin and A. Vinayak, IntechOpen, Rijeka, 2022, ch. 1, DOI: [10.5772/intechopen.101702](https://doi.org/10.5772/intechopen.101702).
- 85 A. P. G. Kieboom, *Recl. Trav. Chim. Pays-Bas*, 1988, **107**, 685–685.
- 86 O. V. Dolomanov, L. J. Bourhis, R. J. Gildea, J. A. Howard and H. Puschmann, *J. Appl. Crystallogr.*, 2009, **42**, 339–341.
- 87 G. M. Sheldrick, *Acta Crystallogr., Sect. A: Found. Adv.*, 2015, **71**, 3–8.
- 88 G. M. Sheldrick, *Acta Crystallogr., Sect. A: Found. Adv.*, 2015, **71**, 3–8.
- 89 R. Jangir, R. Antony and R. Murugavel, *New J. Chem.*, 2016, **40**, 1004–1013.
- 90 L. Wang, L. Zhu, P. Yin, W. Fu, J. Chen, J. Hao, F. Xiao, C. Lv, J. Zhang, L. Shi, Q. Li and Y. Wei, *Inorg. Chem.*, 2009, **48**, 9222–9235.
- 91 Q.-L. Chen, W. Huang, M.-L. Chen, J. Lin, Z.-X. Cao and Z.-H. Zhou, *RSC Adv.*, 2014, **4**, 26499–26507.
- 92 M.-G. Lv, J.-Q. Zhang, Q.-G. Li, K. Gao, S. Andra, Z.-Z. Li, H.-J. Lun and Y.-M. Li, *Cryst. Growth Des.*, 2024, **24**, 5116–5124.
- 93 A. Rahmani and H. Farsi, *RSC Adv.*, 2020, **10**, 39037–39048.
- 94 W. Wei, K. Yu, Z.-h. Su, Y. Yu, B.-b. Zhou and C.-c. Zhu, *Inorg. Chem. Commun.*, 2012, **17**, 21–25.
- 95 M. Alshammari, K. Alshammari, S. Alhassan, A. H. Alshammari, T. Alotaibi, A. Iraqi and T. A. Mohaymen Taha, *Int. J. Hydrogen Energy*, 2024, **67**, 33–41.
- 96 Y.-Q. Lan, S.-L. Li, X.-L. Wang, K.-Z. Shao, D.-Y. Du, H.-Y. Zang and Z.-M. Su, *Inorg. Chem.*, 2008, **47**, 8179–8187.
- 97 D. Mahesh, P. Sadhu and T. Punniyamurthy, *J. Org. Chem.*, 2016, **81**, 3227–3234.
- 98 M. Rostaminasab, A. Rezaeifard, M. Jafarpour and A. Klein, *ACS Appl. Nano Mater.*, 2023, **6**, 22459–22470.
- 99 R. Ferdousian, F. K. Behbahani and B. Mohtat, *Inorg. Nano-Met. Chem.*, 2024, **54**, 1–10.